

Application of ℓ_p -regularized Least Squares For $0 \leq p \leq 1$ in Estimating Discrete Spectrum of Relaxations For Electromagnetic Induction Responses

Mu-Hsin Wei^a, Waymond R. Scott^a, Jr., James. H. McClellan^a, and Gregg D. Larson^b

^a School of Electrical and Computer Engineering;

^b School of Mechanical Engineering

Georgia Institute of Technology, Atlanta, Georgia 30332

ABSTRACT

Broadband EMI sensors have been shown to be capable of detecting and discriminating mines and subsurface explosive objects. It is advantageous to model the EMI frequency response of a target in terms of a discrete spectrum model (or equivalently a sum of real exponentials in the time domain) that is valuable in discrimination. However, in practice it is difficult to obtain the model parameters from measurements. We previously proposed a constrained linear method that can robustly estimate the model parameters when they are nonnegative. In this paper, we present a modified ℓ_p -regularized least squares algorithm, for $0 \leq p \leq 1$, that eliminates the nonnegative constraint. Using synthesized data and lab measurements, the proposed spectrum estimation method is shown to be effective. The results suggest that the proposed method can be used to obtain spectrum of targets for discrimination. We also propose a regularization parameter selection rule for the ℓ_p minimization.

Keywords: Electromagnetic induction (EMI), discrete spectrum of relaxation frequencies (DSRF), sum of exponentials, ℓ_1 minimization, target discrimination, detection

1. INTRODUCTION

Recent research has shown the use of broadband electromagnetic induction (EMI) sensors together with advanced signal processing are capable of discriminating between certain types of buried targets.^{1,2} In discrimination, it is advantageous to model the EMI response as a sum of real exponentials in the time domain or, equivalently, a discrete spectrum model in the frequency domain. Since the relaxation frequencies in the model are invariant to the target's relative orientation and position to the sensor, they can be used as a stable feature of a target.

The EMI frequency response $H(\omega)$ of a metallic target can be expressed as:³

$$H(\omega_n) = c_0 + \sum_{k=1}^K \frac{c_k}{1 + j\omega_n/\zeta_k}, \quad n = 1, 2, \dots, N \quad (1)$$

where c_0 is the shift, K the model order, c_k the real spectral amplitudes, ζ_k the relaxation frequencies, and ω_n the frequencies at which $H(\omega)$ is sampled. The parameter set $S = \{(\zeta_k, c_k) : k = 1 \dots K\}$ is called the Discrete Spectrum of Relaxation Frequencies (DSRF) or simply the spectrum; each pair (ζ_k, c_k) is one relaxation.

It is difficult in practice, however, to obtain the spectral parameters ζ_k and c_k from a given $H(\omega)$. The primary difficulty comes from when the model order K is unknown, the number of measurements N is small, or the model parameters must be real. Most existing methods require a good guess of K for the estimation process to converge. But prior knowledge of K is usually unavailable. Even when the estimation process does converge, the estimates could be far from the true values.⁴ In addition, existing methods may return complex estimates that lack of physical meaning. We previously proposed a constraint linear method that can robustly estimate DSRFs that are free from the difficulties described above.⁵ The method however presumes nonnegative spectra for the targets.

Further author information: (Send correspondence to Mu-Hsin Wei)
Mu-Hsin Wei: E-mail: m.wei@gatech.edu

In this paper, we propose a more general estimation method using ℓ_p -regularized least squares ($0 \leq p \leq 1$) that can estimate spectra consisting of relaxations of mixed signs (bipolar). This proposed method first samples a range of relaxation frequencies, then linearize the estimation problem, and finally solve the problem using an approximated ℓ_p -regularized least squares. As argued by Chartrand, more accurate estimates may be obtained using $p < 1$ than $p = 1$.⁶ The ℓ_p minimization involves selecting a regularization parameter, which is also discussed in this paper. As with the previously proposed constrained optimization method, the ℓ_p method proposed here always returns real model parameters and is stable under noise.

The proposed method is found to be effective from tests on synthetic and laboratory data under various noise levels. Estimating the DSRF from field data also demonstrates that the proposed method can be used in practice. In the future, more work can be done on developing target discrimination algorithms based on the estimated DSRF. In addition, more work can be put into creating a better selection rule for the regularization parameter.

2. ESTIMATION METHOD

The usual approach to estimating the DSRF (i.e., the ζ_k and c_k) is to perform a nonlinear iterative search. However, we follow the strategy of basis pursuit that linearizes the estimation problem by sampling the relaxation frequencies.⁷ The estimation problem then becomes

$$\begin{bmatrix} H(\omega_1) \\ H(\omega_2) \\ \vdots \\ H(\omega_N) \end{bmatrix} = \underbrace{\begin{bmatrix} 1 & \frac{1}{1+j\omega_1/\tilde{\zeta}_1} & \frac{1}{1+j\omega_1/\tilde{\zeta}_2} & \cdots & \frac{1}{1+j\omega_1/\tilde{\zeta}_M} \\ 1 & \frac{1}{1+j\omega_2/\tilde{\zeta}_1} & \frac{1}{1+j\omega_2/\tilde{\zeta}_2} & \cdots & \frac{1}{1+j\omega_2/\tilde{\zeta}_M} \\ \vdots & \vdots & \vdots & \ddots & \vdots \\ 1 & \frac{1}{1+j\omega_N/\tilde{\zeta}_1} & \frac{1}{1+j\omega_N/\tilde{\zeta}_2} & \cdots & \frac{1}{1+j\omega_N/\tilde{\zeta}_M} \end{bmatrix}}_{\tilde{\mathbf{Z}}} \begin{bmatrix} \tilde{c}_0 \\ \tilde{c}_1 \\ \tilde{c}_2 \\ \vdots \\ \tilde{c}_K \end{bmatrix} + error$$

$$\mathbf{h} = \tilde{\mathbf{Z}}\tilde{\mathbf{c}} + error \quad (2)$$

where $\tilde{\zeta}_m$ are the *sampled* relaxation frequencies, \tilde{c}_m the corresponding spectral amplitude estimators, \mathbf{h} the observation vector, and $\tilde{\mathbf{Z}}$ the overcomplete dictionary. $\tilde{\mathbf{c}}$ is the weighted selector vector containing the shift estimator \tilde{c}_0 followed by the spectral amplitude estimators. We expect the solution for $\tilde{\mathbf{c}}$ to have many zero elements because $M \gg K$, i.e., $\tilde{\mathbf{c}}$ will be sparse.

The sampled ζ are generated by enumerating a large set of M *possible* relaxation frequencies uniformly distributed in the log- ζ space ($M \gg K$). While Austin *et al.* suggests sampling based on the Fisher information of the model,⁸ we found that uniform sampling produces a very similar set of sampled ζ . The uniform sampling, however, is simpler.

Since $\tilde{\mathbf{c}}$ is sparse, we estimate it using the ℓ_p -regularized least squares technique, for $0 \leq p \leq 1$, because it promotes sparse solutions.⁹ The objective function is

$$\arg \min_{\tilde{\mathbf{c}}} \|\tilde{\mathbf{Z}}'\tilde{\mathbf{c}} - \mathbf{h}'\|_2^2 + \lambda \|\tilde{\mathbf{c}}\|_p^p, \quad 0 \leq p \leq 1 \quad (3)$$

$$\text{where } \tilde{\mathbf{Z}}' = \begin{bmatrix} \Re(\tilde{\mathbf{Z}}) \\ \Im(\tilde{\mathbf{Z}}) \end{bmatrix}, \quad \mathbf{h}' = \begin{bmatrix} \Re(\mathbf{h}) \\ \Im(\mathbf{h}) \end{bmatrix},$$

and λ is the regularization parameter. Separating the real and imaginary parts in $\tilde{\mathbf{Z}}$ makes the whole system real and produces only real estimates. Ideally, in the optimal $\tilde{\mathbf{c}}$, only those \tilde{c}_m with corresponding $\tilde{\zeta}_m$ that are near a true ζ_k will be nonzero, and they will take on the correct spectral amplitudes c_k . It follows that a DSRF can then be deduced from the nonzero estimated \tilde{c}_m and their corresponding $\tilde{\zeta}_m$.

The ℓ_p -regularized least squares solution for $p < 1$ can be approximated by an iteratively reweighted ℓ_1 algorithm proposed by Candès *et al.*⁹ The weights are updated as suggested in Ref. 10. We also adopt the ϵ -regularization technique used in the same paper. In summary, (3) is approximated by (see also Ref. 11):

Algorithm 1: Approximated ℓ_p -regularized least squares

Input: $\tilde{\mathbf{Z}}', \mathbf{h}', p, \lambda, \tilde{\mathbf{c}}^0$
1 $\tilde{\mathbf{c}}^n \leftarrow \tilde{\mathbf{c}}^0$
2 **for** $k \leftarrow 0$ **to** -8 **step** -1 **do**
3 $\epsilon \leftarrow 10^k$
4 **repeat**
5 $\tilde{\mathbf{c}}^{n-1} \leftarrow \tilde{\mathbf{c}}^n$
6 $w_i^n \leftarrow (|\tilde{c}_i^{n-1}| + \epsilon)^{p-1}$
7 $\tilde{\mathbf{c}}^n \leftarrow \arg \min \|\tilde{\mathbf{Z}}' \tilde{\mathbf{c}} - \mathbf{h}'\|_2^2 + \lambda \sum_{i=1}^{M+1} w_i^n |\tilde{c}_i|$
8 **until** $\|\tilde{\mathbf{c}}^n - \tilde{\mathbf{c}}^{n-1}\|_2 < \sqrt{\epsilon}/100$
9 **return** $\tilde{\mathbf{c}}^n$

The ℓ_1 minimization problem in step 7 is solved by `l1_ls`, a MATLAB optimizer proposed by Kim *et al.*¹² We have also found that normalizing the input data \mathbf{h} , as well as the columns of $\tilde{\mathbf{Z}}'$, to have unit ℓ_2 norm increases the accuracy of estimation. Setting entries of $\tilde{\mathbf{c}}^0$ to all ones also seems to be effective. However, the solution is insensitive to the initial value of $\tilde{\mathbf{c}}^0$. It can also be set to other values such as the solution to $\min \|\tilde{\mathbf{Z}}' \tilde{\mathbf{c}} - \mathbf{h}'\|_2$.¹⁰ The nonzero entries of $\tilde{\mathbf{c}}$ selected by (3) along with the corresponding $\tilde{\zeta}_m$ are the relaxations needed in the estimated DSRF, $\hat{S} = \{(\hat{\zeta}_l, \hat{c}_l) : l = 1 \dots L\}$.

3. ESTIMATION RESULTS

The proposed estimation method is tested on synthetic, laboratory, and field data to show its functionality, accuracy, and stability. The hardware system used is a wideband EMI sensor operating at 21 frequencies approximately logarithmically distributed over the range 300 Hz–90 kHz (2.5 decades).¹³ The synthetic data is generated in accordance with the hardware specification. The range of ζ for estimation is chosen such that $\log(\tilde{\zeta}_{\min})$ and $\log(\tilde{\zeta}_{\max})$ are 2.45 and 6.62, respectively, i.e., 4.17 decades.

All estimations are performed with $M = 100$,⁵ and all presented spectra are normalized such that $\sum |c_i| = 1$. Spectral amplitudes less than 10^{-5} are not displayed. Unless specified, $p = 0.5$ is chosen as a representative case. The regularization parameter λ is chosen based on the method described in Section 4. Results presented in this section may achieve higher accuracy with a more sophisticated λ selection rule. Here we demonstrate the usability of the proposed algorithm with a simple λ selection rule. See Section 4 for more discussion on the choice of λ .

3.1 Dissimilarity Measure Between Two DSRFs

In order to evaluate the goodness of the estimated DSRF, we need to define a measure of dissimilarity that is appropriate for sparse spectra with multiple peaks. We use the Earth Mover’s Distance (EMD)¹⁴ which quantifies the “amount of work” to morph one spectrum into the other. Strictly speaking the EMD is only defined for positive spectra, but we can account for negative spectral amplitudes by defining the distance function between two relaxations (ζ_i, c_i) and $(\hat{\zeta}_j, \hat{c}_j)$ to be:

$$d_{ij} = \begin{cases} |\log \zeta_i - \log \hat{\zeta}_j| & , c_i \hat{c}_j \geq 0 \\ 1 + |\log \zeta_i - \log \hat{\zeta}_j| & , c_i \hat{c}_j < 0 \end{cases}$$

which penalizes relaxations with different signs. The penalization can be defined differently as suitable. Spectra are made nonnegative and normalized ($\sum |c_i| = 1$) prior to the EMD computation. Finally, notice that the EMD is measured in decades because it is examined in \log - ζ space.

3.2 Synthetic Six-relaxation DSRF

We test the proposed ℓ_p method (using $p = 0.5$) on a six-relaxation DSRF synthesized at 70 dB SNR with additive white Gaussian noise (Fig. 1). This is a case that cannot be handled by traditional nonlinear parameter optimization,⁴ or the nonnegative linear method.⁵ Though shifted slightly, all six relaxation frequencies are recovered by using **Algorithm 1**. The estimation result is satisfactory because the model parameters are real and the deviation from the truth is small. The EMD between the estimated and the true DSRF is 0.15 decades. There is one extra relaxation near $\log\zeta=2$ in the estimated spectrum, but it has a small amplitude and can be neglected.

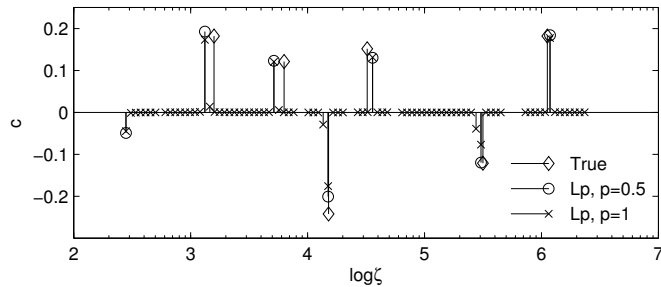


Figure 1: Theoretical and estimated DSRF of a six relaxation target.

The same spectrum is also estimated with $p = 1$ using `l1_ls`. In this case, many extra relaxations are introduced by the fitting process (Fig. 1). However, because the extra relaxations are very small in amplitude, the EMD is still small – 0.16 decades. Real targets are not likely to have a spectrum with many small relaxations around a strong relaxation. In fact, Baum argues that physical relaxation frequencies are discrete.³ However, the small relaxations introduced by $p = 1$ seem to give a continuous spectrum of relaxation frequencies. In this sense, $p < 1$ gives a sparser solution that more accurately resembles the expected physical spectrum even though this may not always be reflected in the EMD measure.

3.3 Signal to Noise Ratio

To see how the proposed method performs in noise, a Monte Carlo simulation versus SNR is performed. The true spectrum is from a target with a four-relaxation DSRF including negative relaxations. The simulation result shows the robustness of the estimation method at different SNRs (Fig. 2). The EMD between the estimate and the truth increases as the SNR decreases. This suggests that the proposed method is usable in a range of SNR where the EMD is below some threshold. This threshold, however, depends on the application of the estimated spectrum. For example, if the DSRFs are used as features for classification, a more robust classifier may tolerate worse estimations and, therefore, allow lower SNR. For our purpose, spectra with an EMD below 0.1 are considered visually similar, those with an EMD above 0.2 exhibit visual differences, but may still resemble each other. Thus, we consider 50 dB as the threshold SNR. In our laboratory measurements, a typical SNR for loop targets is 70 dB.

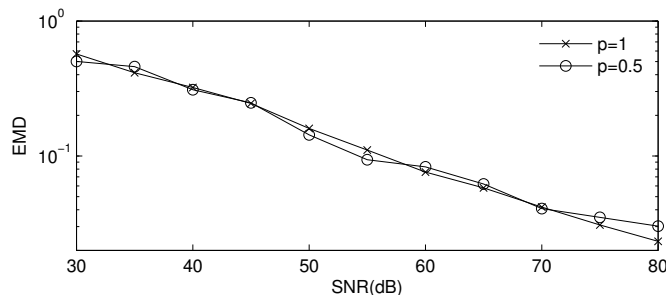


Figure 2: Monte Carlo simulation on goodness of estimation vs. SNR. Sample size is 100 per SNR.

3.4 Laboratory Data

We verify the functionality of the estimation method on laboratory data where we know the theoretical DSRF. An automated, non-metallic measurement facility is used to measure EMI responses of a target at various positions and orientations relative to the sensor.¹⁵ We observe that the proposed method is effective with laboratory data.

A target that consists of three mutually orthogonal copper loops is examined. The loop diameters and thickness are 3/20, 4/30, and 5/36, respectively in cm/AWG(American Wire Gauge). We pick a specific orientation and position relative to the EMI sensor that best shows the existence of bipolar relaxation amplitudes in a spectrum. The target frequency response of this configuration is shown in Fig. 3a, the SNR was estimated to be 38 dB, and its estimated DSRF in Fig. 3b. Theoretical data are also displayed. We see that the estimate and theory agree well, and the EMD between the theoretical and estimated DSRF is 0.10 decades.

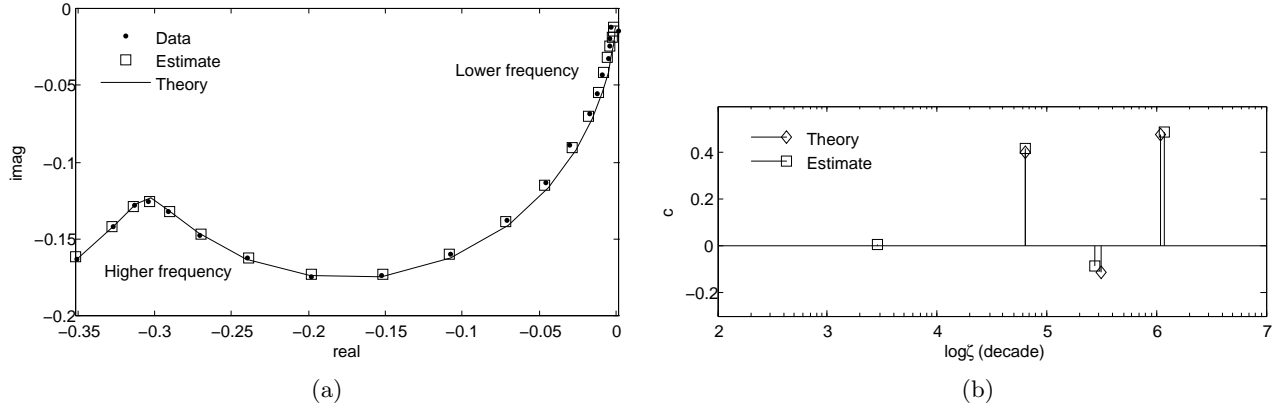


Figure 3: (a) Frequency response of three mutually orthogonal copper loops. The frequency response is normalized such that $\|\mathbf{h}\|_2 = 1$. (b) Theoretical and estimated DSRF of the response in (a).

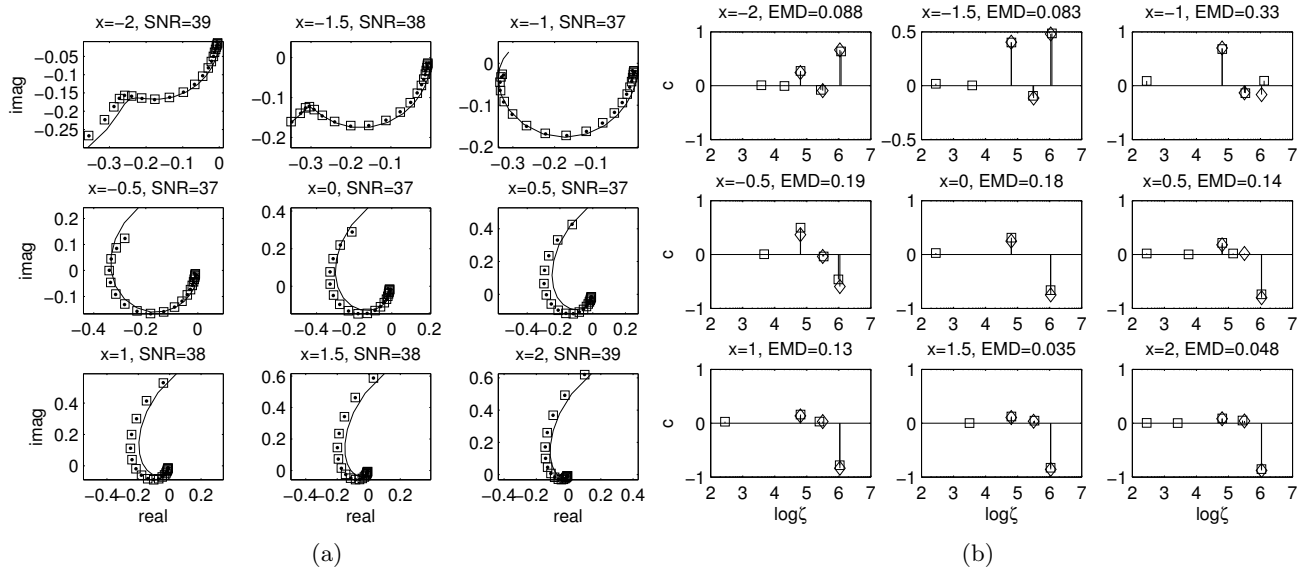


Figure 4: The plots share the same annotation as Fig. 3. (a) Frequency responses of the three mutually orthogonal copper loops at nine different x locations. (b) Theoretical and estimated DSRF of the corresponding responses in (a). The SNR is measured in dB, x positions in cm, and EMD in decades.

Next we examine the changes in the DSRF as the target moves relative to the EMI sensor. The same target configured at a fixed orientation is displaced at different positions along a horizontal axis (x). The vertical distance between the target and sensor is 6 cm. The EMI sensor is located at $x = 0$. Overall, the theory and measurement agree (Fig. 4).

As expected from the theory, while the frequency response changes dramatically as the target moves along the x axis, the corresponding change in the spectral domain only occurs in the spectral amplitudes. The three dominant relaxation frequencies remain unchanged. The proposed method successfully estimates the spectra that agree with this phenomenon. All three relaxation frequencies are consistently estimated. The extra relaxations all have small amplitudes that can be safely ignored. This invariant property of the relaxation frequencies makes the DSRF valuable especially for target discrimination.

3.5 Field Data

Here we demonstrate the functionality of the proposed method when applied to field data. From the consistency of the estimated DSRF, we suggest that these spectra can indeed be used as features for target discrimination. The proposed method is applied to three types of landmines. For each type of mine, measurements were collected from several mines buried at different depths and locations.

When estimating the DSRF from field data, we observe that the estimation method sometimes returns a single relaxation at ζ_1 or ζ_M (the endpoints of the sampled ζ domain), as we saw in the estimate in Fig. 1. This artifact could be easily removed manually or by a weighted least squares term. For this section, we adopt the latter approach to eliminate estimated relaxations at endpoints. This is simply done by replacing $\tilde{\mathbf{Z}}$ and \mathbf{h} in Eq. (3) with $\tilde{\mathbf{Z}}_w$ and \mathbf{h}_w , respectively, where

$$\begin{aligned}\tilde{\mathbf{Z}}_w &= W\tilde{\mathbf{Z}}, \\ \mathbf{h}_w &= W\mathbf{h},\end{aligned}$$

and W is a diagonal matrix with weights $[w_1, w_2, \dots, w_N]$ on the diagonal. To discourage over fitting at endpoints, we put less weight on the highest and lowest frequencies.

Using the weighted method, the DSRF of each sample was estimated and then plotted together with others of the same type (Figs. 5–7). For all three types of mine, the estimated DSRFs have consistent shapes. The relaxations that appear to be inconsistent are small in amplitude. For each type of mine the stronger relaxations share the same relaxation frequencies. While the true spectra of these field targets are unknown, from the consistency of the estimated spectrum, we have good faith that what is obtained is accurate. Various simulations and laboratory results from previous sections also support this view.

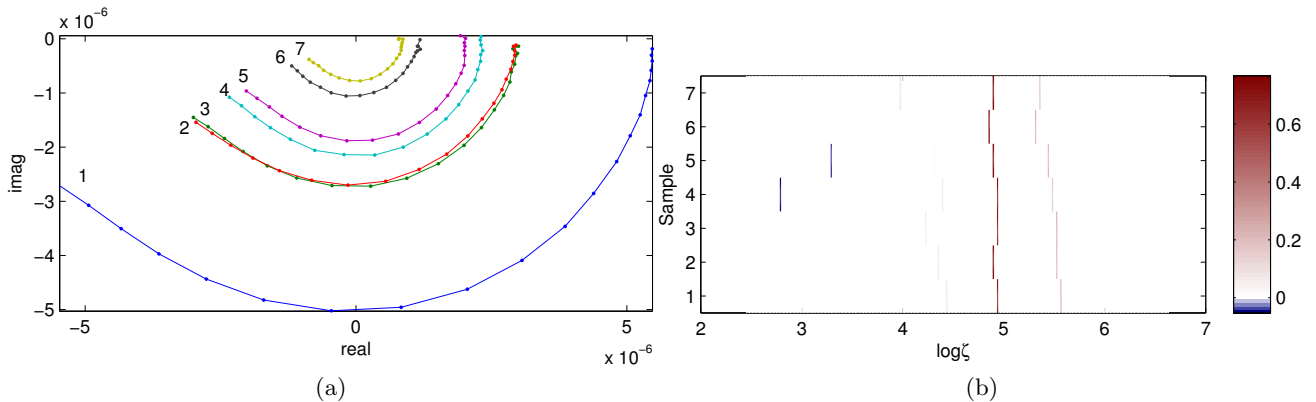


Figure 5: Frequency responses and estimated DSRFs of seven Type-I mines: a low-metal content, magnetic, weak EMI response antipersonnel mines. The SNR ranges from about 20 dB to 35 dB. (a) Raw frequency responses. (b) Estimated DSRFs. The spectral amplitude is represented by the color intensity.

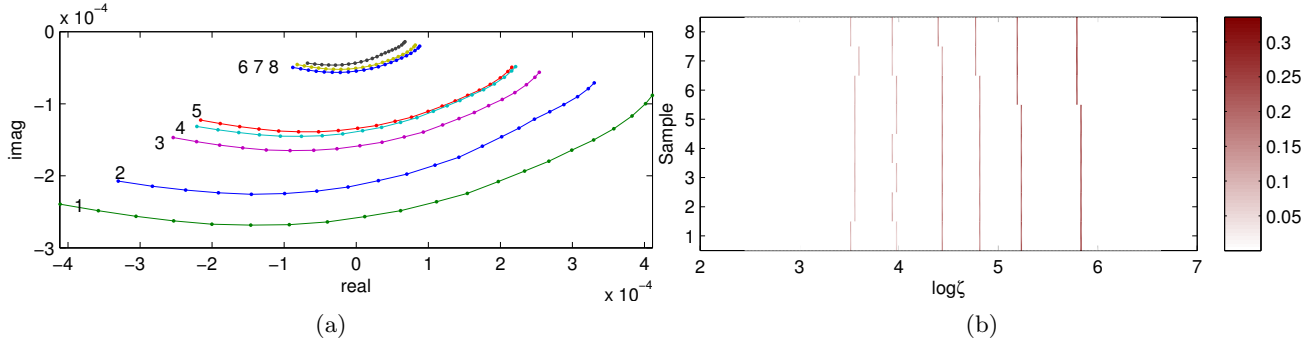


Figure 6: Frequency responses and estimated DSRFs of eight Type-II mines: a medium-metal content, magnetic, strong EMI response antipersonnel mine. The SNR ranges from about 55 dB to 70 dB. (a) Raw frequency responses. (b) Estimated DSRFs. The spectral amplitude is represented by the color intensity.

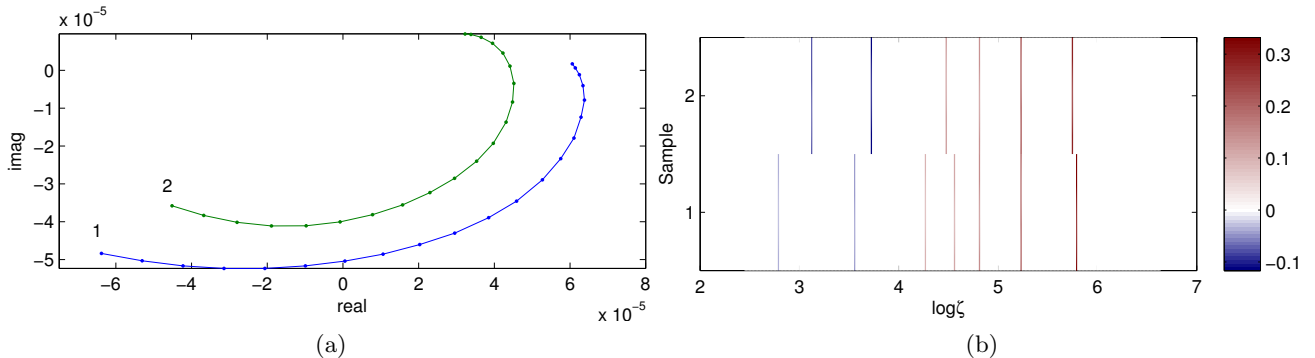


Figure 7: Frequency responses and estimated DSRFs of two Type-III mines: a medium-metal content, strong EMI response antipersonnel mine. The SNR is around 50 dB. (a) Raw frequency responses. (b) Estimated DSRFs. The spectral amplitude is represented by the color intensity.

4. CHOOSING λ

In this section, we examine the behavior of the proposed method in relation to the regularization parameter λ . We observe that the optimal λ that gives the minimum estimation error is quasi independent of the model order and has a simple relation to the SNR. We propose a simple λ selection formula that exploits this observation. All discussions and figures presented here assume $p = 0.5$ unless otherwise specified.

To understand how the goodness of estimation changes with λ and SNR, we conduct a cross-validation-like simulation. First, we build a collection of synthetic spectra with different model orders and a variety of distributions of relaxations. For each spectrum at a fixed SNR, the spectrum is estimated 100 times for each λ within a range, and the average goodness of fit, measured by the EMD between the available truth and the estimate, is recorded. This is done for a range of SNRs.

The simulation result (Fig. 8a) shows that for each model order the EMD (error) surface is well-behaved (i.e., smooth) with respect to the SNR and λ . Moreover, the surfaces are convex-shaped, implying that the minimum EMD is achievable by a unique λ for a specific model order and SNR. The wide valley of the surface also shows that the goodness of estimation is not very sensitive near the optimal λ .

On the other hand, we observe that for all model orders, the near-minimum EMD (the valley of the surfaces) occur in about the same SNR- λ region. This means that a single optimal selection rule may be applicable for all model orders. We confirm that this is possible when we average the EMD surfaces of different model orders (Fig. 8b). The averaged surface still exhibits all properties of a single model order surface - smooth, convex, and wide valley. From the averaged surface, we observe that using only the SNR value, we can pick a λ that is near optimal for all model orders. Tracing out the optimal λ at each SNR, we find that the optimal λ curve is almost linear (Fig. 8b). Then, intuitively, we approximate the optimal λ with a semilog function of SNR. This is done

by fitting the optimal $\log\text{-}\lambda$ curve with a linear function. Weights may be added to promote certain SNR's that are more important.

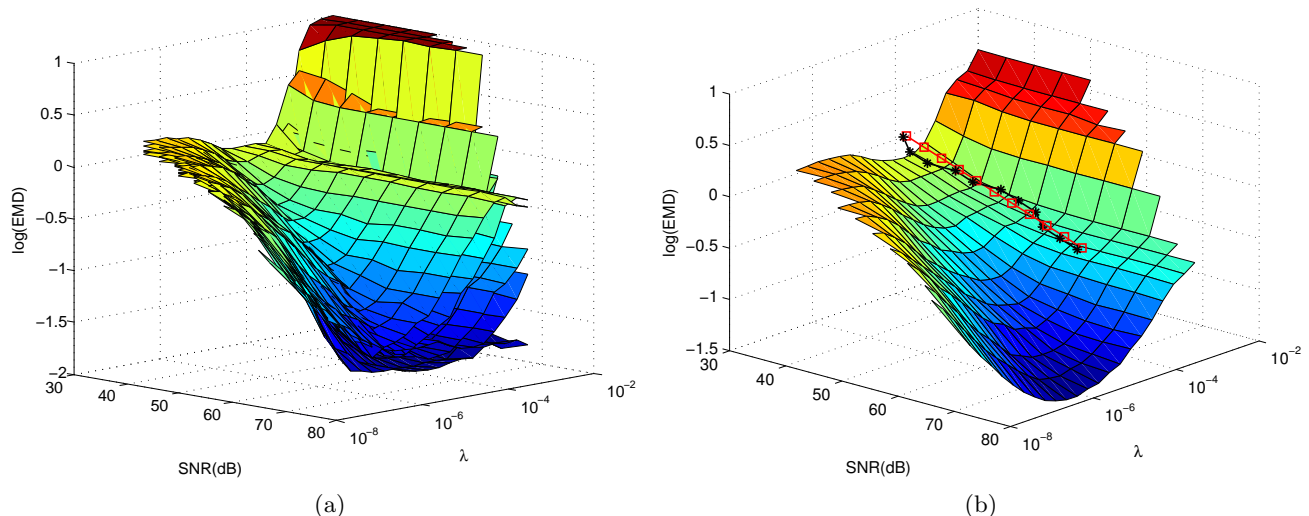


Figure 8: (a) Monte Carlo simulation of the goodness of estimation (EMD) of spectra of different model orders (one to six). Each spectrum constitutes one surface in the figure. (b) Average of EMD surfaces in (a). The curve with asterisk markers traces out the optimal λ 's. The line with square markers approximates the optimal λ 's.

For our problem setup, the λ is chosen by (also shown in Fig. 8b)

$$\log \lambda = -0.05 \cdot \text{SNR} - 2.2 \quad (4)$$

Since the surface has a wide-valley, the resulting λ selection rule is near-optimal as long as it lies in the valley, which is true in this case. In practice, this $\log\text{-}\lambda$ selection rule that is linear in SNR allows the regularization parameter to be determined with negligible computation time. When processing the laboratory data, we use (4) along with an estimate of the SNR to determine λ for use in **Algorithm 1**. The same empirical method can be repeated for other p 's, and the result is also a linear relationship between $\log \lambda$ and SNR.

ACKNOWLEDGMENTS

This work is supported in part by the US Army REDCOM CERDEC Night Vision and Electronic Sensors Directorate, Science and Technology Division, Countermine Branch and in part by the U. S. Army Research Office under Contract Number W911NF-05-1-0257.

REFERENCES

- [1] Gao, P., Collins, L., Garber, P. M., Geng, N., and Carin, L., "Classification of landmine-like metal targets using wideband electromagnetic induction," *IEEE Trans. Geosci. Remote Sens.* **38**, 1352–1361 (May 2000).
- [2] Fails, E. B., Torrione, P. A., Scott, Jr., W. R., and Collins, L. M., "Performance of a four parameter model for modeling landmine signatures in frequency domain wideband electromagnetic induction detection systems," *Proc. SPIE* **6553**, 65530D (Apr. 2007).
- [3] Baum, C. E., "On the singularity expansion method for the solution of electromagnetic interaction problems," Interaction Notes 88, Air Force Weapons Laboratory (1971).
- [4] Das, Y. and McFee, J. E., "Limitations in identifying objects from their time-domain electromagnetic induction response," *Proc. SPIE* **4742**, 776–788 (Apr. 2002).
- [5] Wei, M., Scott, Jr., W. R., and McClellan, J. H., "Robust estimation of the discrete spectrum of relaxations for electromagnetic induction responses," *IEEE Trans. Geosci. Remote Sens.* **48**, 1169–1179 (Mar. 2010).

- [6] Chartrand, R., “Exact reconstruction of sparse signals via nonconvex minimization,” *IEEE Signal Process. Lett.* **14**(10), 707–710 (2007).
- [7] Chen, S. S., Donoho, D. L., and Saunders, M. A., “Atomic decomposition by basis pursuit,” *SIAM Review* **43**(1), 129–159 (2001).
- [8] Austin, C. D., Ertin, E., Ash, J. N., and Moses, R. L., “On the relation between sparse sampling and parametric estimation,” *Proc. DSP Workshop*, 387–392 (Jan. 2009).
- [9] Candès, E. J., Wakin, M. B., and Boyd, S. P., “Enhancing sparsity by reweighted ℓ_1 minimization,” *J. Fourier Anal. Appl.* **14**(5), 877–905 (2008).
- [10] Chartrand, R. and Yin, W., “Iteratively reweighted algorithms for compressive sensing,” *Proc. ICASSP*, 3869–3872 (Mar. 2008).
- [11] Figueiredo, M. A. T. and Nowak, R. D., “A bound optimization approach to wavelet-based image deconvolution,” *Proc. ICIP* **2**, 782–785 (2005).
- [12] Kim, S. J., Koh, K., Lustig, M., and Boyd, S., “An efficient method for compressed sensing,” *Proc. ICIP* **3**, 117–120 (2007).
- [13] Scott, Jr., W. R., “Broadband array of electromagnetic induction sensors for detecting buried landmines,” *Proc. IGARSS* (July 2008).
- [14] Rubner, Y., Tomasi, C., and Guibas, L. J., “A metric for distributions with applications to image databases,” *Proc. ICCV*, 59–66 (Jan. 1998).
- [15] Larson, G. D. and Scott, Jr., W. R., “Automated, non-metallic measurement facility for testing and development of electromagnetic induction sensors for landmine detection,” *Proc. SPIE*, 73030X (Apr. 2009).